FRACTIONAL DYNAMICS FOR QUANTUM RANDOM WALKS*

HARBIR ANTIL† AND LUCAS BOUCK‡

Abstract. Quantum random walks (QRWs) are important tools for the development of algorithms in the growing field of quantum computing. The standard partial differential equation (PDE) based models of QRWs fail to capture the peaks of QRW dynamics, which is important for quantum computing algorithms. This paper introduces a new fractional PDE model of a QRW. The resulting model is the time-Fractional Fokker-Planck PDE. We develop an algorithm to compute numerical solution to this PDE and provide an optimization algorithm to compute the optimal exponent for the fractional time derivative. The numerical results clearly illustrate a better match between the fractional models and discrete QRW dynamics.

Key words. quantum random walks, Hadamard random walk, quantum computing, space-time continuous model, inverse problems, optimal fractional exponent.

AMS subject classifications. 68Q12, 81P94, 81P68, 34K37, 42A38, 35Q93, 80M50, 31A25,

s:intro

1. Introduction.

Quantum computing is a new and fast growing field. Indeed harnessing of Quantum states and manipulating and controlling their behavior at atomic and subatomic scales has been recently identified as one of National Science Foundation's Big Ideas [15]. Quantum computing demonstrates potential in greatly increasing computing power for several problems in computer science. One such example of importance of quantum computing is Shor's algorithm, which has led to an algorithm for quantum computers to find the prime factorization of integers efficiently [25]. The latter is a significant challenge in computer science. Physical implementation still lags behind theory, but physical quantum computers can prime factorize, for instance, 15 using Shor's algorithm [29].

The focus of this paper is on the specific set of tools for quantum computing known as quantum random walks (QRWs). QRWs can be used in many algorithms such as element distinctness algorithms [2] or search algorithms [24]. Both the continuous [13] and discrete [19] time quantum random walks (QRWs) have shown promise to serve as universal models of computation. The paper [30] provides a detailed review of the area of QRWs.

There are two main formulations of QRWs. The first involves discrete space and continuous time. Such a random walk can be described in terms of a walker moving on a graph, $G = (V, E)$, where $V = \{v_j\}_{j=1}^n$ is a set of vertices and $n = |V|$ is the number of vertices. The state of the random walk is described by a vector $\psi \in \mathbb{C}^n$, where the j^{th} component of ψ is the probability amplitude of being at the vertex v_j. The evolution of the walk is defined by Schrödinger's equation $i\frac{\mathrm{d}}{\mathrm{d}t}\psi = \gamma L\psi$, where $\gamma > 0$ is a diffusion coefficient and the $n \times n$ matrix L is the graph Laplacian. For a more detailed explanation and review of the literature on continuous time discrete space QRWs, we refer to [30, Sec. 2.4].

The second formulation is also defined on a graph (in terms of spatial variable), but instead of being continuous time, it is discrete in time. Despite the clear differences between these two QRWs, it has been shown in [14] that the continuous time limit

*The work of the first author is partially supported by NSF grant DMS-1521590. The work of second author is partially supported by NSF grant DMS-1407087.

†Department of Mathematical Sciences, George Mason University, Fairfax, VA 22030, USA. hantil@gmu.edu

‡Department of Mathematical Sciences, George Mason University, Fairfax, VA 22030, USA. lbouck@gmu.edu

of discrete quantum random walks yield continuous time random walks on arbitrary graphs.

The focus of this paper is to introduce a new fractional partial differential equation (PDE) based continuous space-time model for the so-called discrete Hadamard QRW (cf. section 2). Previous work in [8] also considered a continuous space-time model of the discrete Hadamard QRW. We shall see that the aforementioned model in [8] is a special case of our new fractional model. Our numerical experiments suggests that [8] fails to capture the discrete Hadamard QRW dynamics (see Figure 2). On the other hand, our fractional model can capture these to a significantly high accuracy (see Figure 5). The continuous space-time models are indispensable to the mesh independent algorithms. The idea of mesh independence in image processing has been quite successfully argued in [12, Sec. 1], see also [4] for optimal control problems. The PDE based models for QRWs will allow for a plethora of PDE techniques to be used for algorithms that rely on QRWs. In addition, it allows us to create mesh-independent algorithms. The discrete QRW will naturally arise after a discretization of the PDE model for QRW and can be subject to the analysis of the PDE.For the success of such a research program we must first ensure that our continuous PDE based model captures the discrete QRW dynamics. The goal of this paper is to introduce such a PDE based model.

Besides this we also introduce an optimization problem to determine the fractional exponent (order of the fractional time-derivative) in the model. Notice that this is an inverse problem. Even though problems to determine the fractional exponent on diffusion operator (Laplacian, for instance) have been considered in the literature earlier [26], but to the best of our knowledge this is the first place where such an identification problem has been considered, and applied to a realistic problem, for the fractional time derivative.

The rest of the paper is organized as follows. In Section 2 we first describe the discrete Hadamard QRW. Section 3 will give a brief introduction of the necessary fractional calculus. In Section 4, we provide a detailed motivation of the fractional PDE based model for QRWs. In Section 5, a numerical method for solving the fractional model is outlined, and Section 6 provides a convergence study of the numerical scheme. We outline an optimization algorithm to determine the optimal order of the fractional derivative in Section 7 and present the numerical results in Section 8.

s:Hadamard

2. Discrete Hadamard QRW.

The this section we will describe the formulation of what is known as the discrete Hadamard walk. This is the walk that is under consideration in this paper. A more detailed explanation and additional theoretical results can be found in [30, Sec. 2.2].

The state of a generic QRW is described as a tensor product of two complex vectors $\mathbf{c} \otimes \mathbf{p} \in \mathcal{H}_c \otimes \mathcal{H}_p$. The two dimensional Hilbert space $\mathcal{H}_c$ is the coin space and has an orthonormal basis $\{\mathbf{w}_0, \mathbf{w}_1\}$. The (coordinate-) vector $\mathbf{c}$ contains probability amplitudes as we will discuss below. The infinite dimensional Hilbert space $\mathcal{H}_p$ is the position space and also has an orthonormal basis $\{\mathbf{v}_i\}_{i\in\mathbb{Z}}$ with $\mathbb{Z}$ denoting the set of integers. For this paper, the basis vectors for the position space can be interpreted as positions along a line. For example, $\mathbf{v}_0$ corresponds to the center of the line. Let $\mathbf{c} \otimes \mathbf{p} = \sum_{k\in\mathbb{Z}} (a_k \mathbf{w}_0 + b_k \mathbf{w}_1) \otimes \mathbf{v}_k$ be an arbitrary quantum state in $\mathcal{H}_c \otimes \mathcal{H}_p$ then we denote the probability of being at position $k \in \mathbb{Z}$ by $P(k) = |a_k|^2 + |b_k|^2$, where $|\cdot|$ is the complex modulus.

The evolution of the a generic walk is described by the action of two operators: coin operator (C) and shift operator (S). The action of a coin operator C on a coin

state $\mathbf{c}$ is just a matrix-vector product. There are a wide varieties of coin operators, and the primary requirement for C is that it is unitary. For this paper, we will focus on the Hadamard operator, which for the canonical basis, is the matrix

adamard_coin}

$$C = \frac{1}{\sqrt{2}} \begin{pmatrix} 1 & 1 \\ 1 & -1 \end{pmatrix}. \tag{1}$$

Notice that the coin operator C acts on the coin state $\mathbf{c}$. On the other hand, the shift operator S acts on the entire state $\mathbf{c} \otimes \mathbf{p}$ and its action on $\mathbf{c} \otimes \mathbf{p}$ defined as:

ift_operator}

$$S\Big(\sum_{i\in\mathbb{Z}} (a_i \mathbf{w}_0 + b_i \mathbf{w}_1) \otimes \mathbf{v}_i\Big) = \sum_{i\in\mathbb{Z}} (a_{i-1} \mathbf{w}_0 + b_{i+1} \mathbf{w}_1) \otimes \mathbf{v}_i, \tag{2}$$

i.e., the shift operator shifts the coin state's ($\mathbf{c}$) first component to the right and second component to the left.

In addition, every QRW is supplemented with initial conditions. For our paper, we will consider the so-called symmetric initial conditions given by the state vector

hadamard_ic}

$$\mathbf{c} \otimes \mathbf{p} = \frac{1}{\sqrt{2}} \begin{pmatrix} 1 \\ i \end{pmatrix} \otimes v_0. \tag{3}$$

Such an initial condition is called symmetric because the probabilities of the resulting walk are symmetric about position 0, i.e., $P(-k) = P(k)$ for all $k \in \mathbb{Z}$. Figure 1 illustrates one step (a single time iteration) of a quantum walk on a line using the Hadamard coin operator from (1), the shift operator from (2), and the initial conditions from (3).

onal Calculus

3. Fractional Operators. Recently fractional operators have received a tremendous amount of attention especially in physics and engineering applications due to their ability to model anomalous diffusion [20]. Several stochastic models have been introduced in the literature to justify anomalous diffusion: fractional Brownian motion, Lévy flights, Continuous Time Random Walk etc. Fractional dynamical systems can be derived using random walks. There the fractional diffusion (Laplacian) can be derived from a discrete random walk that can experience long jumps [28]. The fractional time derivative ∂_t^α of order $\alpha \in (0, 1)$ is a byproduct of time delays [7] between the jumps.

Fractional models have also emerged as a modeling alternative in many applications due to their ability to capture sharper edges across the interface [3] and their ability to capture the hereditary properties in materials [9]. In the former case one typically uses fractional Laplacian $(-\Delta)^s$ of order $s \in (0, 1)$ and the latter case fractional time derivative ∂_t^α of order $\alpha \in (0, 1)$. Fractional operators are nonlocal operators that can capture multiscale effects, see for instance [10] for the electrical signal propagation in cardiac tissue that has been experimentally validated and [5] for image denoising problems with perfect-reconstruction. We refer to the monograph [23], the papers [22, 1, 16] and their references for more background on the fractional diffusion and the fractional time derivatives.

The focus of this paper is on fractional time derivative based models for QRWs, nevertheless, since our model contains Laplacian one can easily extend our approach and create a fractional space-time version of our model. One way of defining the fractional Laplacian is using the Fourier transform. For example, under sufficient smoothness assumptions on u the fractional Laplacian in $\mathbb{R}^n$ with n being the space dimension can be defined as

$$(-\Delta)^s u(\mathbf{x}, t) = \mathcal{F}^{-1}(|\xi|^{2s} \mathcal{F}(u(\mathbf{x}, t)))$$

amard_example

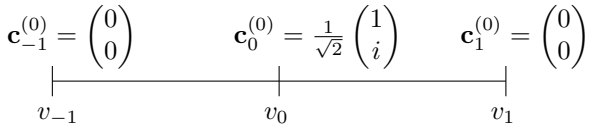

Application of coin operator C

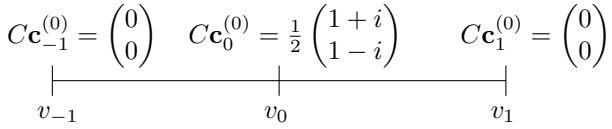

Application of shift operator, S

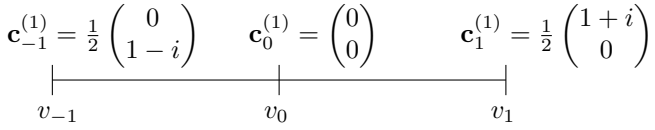

FIG. 1. *Example of one step of a Hadamard walk with symmetric initial conditions. Each step involves the action of a coin and shift operator. For* $\mathbf{c}_k^{(j)}$*, the bottom index means the coin vector position* k *and the top index denotes the time iteration* j*.*

for every $t \in \mathbb{R}_+$. Here ξ is the frequency variable with respect to the spatial variable $\mathbf{x}$. The Fourier definition of $(-\Delta)^s$ preserves some interesting properties, for example, $(-\Delta)^\alpha(-\Delta)^\beta u(\mathbf{x},t) = (-\Delta)^{\alpha+\beta}u(\mathbf{x},t)$. For completeness, we point out that there are several definitions of $(-\Delta)^s$ in $\mathbb{R}^n$ however all of them coincides [21, 11].

Next we will define a fractional time derivative. As in case of fractional Laplacian there are several definitions of fractional time derivatives and they are not equivalent. However we choose to work with Caputo fractional derivative which has been recently used to model plasma turbulance. In addition, it is easy to see that the Caputo fractional derivative of a constant function is zero and a result the time-independent solutions are also solutions to the time-dependent problem. Unfortunately this is not the case with another widely used definition of fractional time derivative - Riemann-Lioville fractional derivative. The Caputo fractional time derivative of order $0 < \alpha < 1$ of a function u is

{fracdef}

$$\partial_t^\alpha u(\mathbf{x},t) = \frac{1}{\Gamma(1-\alpha)} \int_0^t \frac{\partial_t u(\mathbf{x},y)}{(t-y)^\alpha}\, \mathrm{d}y, \tag{4}$$

where ∂_t denotes the standard first time derivative. Notice that it is possible to define Caputo fractional derivative where $\partial_t u$ does not appear explicitly [16]. Both the fractional time derivative and fractional Laplacian are nonlocal operators. This is clear from (4), i.e., in order to evaluate the fractional time derivative of u at time t, we need information about u from 0 to t. This is unlike the standard time derivative, which is a local operator. We further set $\partial_t^\alpha = \partial_t$ when $\alpha = 1$, i.e., we obtain the

standard time derivative.

4. Fractional Model for QRWs. We begin this section by describing the previous work on a continuous space-time PDE model by Blanchard et. al. from [8] to capture the discrete Hadamard QRW. The authors start with discrete Hadamard QRW as described in section 1, i.e., they use the Hadamard coin operator (1), the shift operator (2), and symmetric initial conditions from (3). Then they arrive at the following limiting PDE system (as the discrete space time steps tends to zero)

$$\begin{aligned} \frac{\partial}{\partial s}u(s,y) &= \frac{1}{2}\frac{\partial^2}{\partial y^2}u(s,y) - \frac{\partial}{\partial y}[\tanh(y)u(s,y)], \quad \text{in } (0,\infty)\times\mathbb{R} \\ u(0,y) &= \delta(y), \quad y \in \mathbb{R} \\ \lim_{y\to\pm\infty} u(s,y) &= 0, \quad s \in (0,\infty) \end{aligned} \tag{5}$$

where $s = 2\sqrt{2}t$ and $y = 2x$ with x and t denoting the space and time variables, respectively. Moreover $\delta(y)$ is the Dirac delta function.

We next carry out a comparison between the dynamics of (5) and the discrete Hadamard QRW. The results of our experiment are shown in Figure 2. Here we are

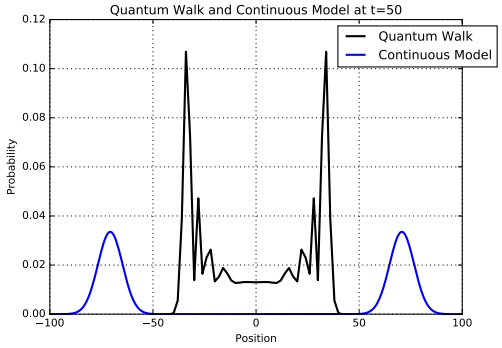

FIG. 2. *A comparison between the probability mass function of the discrete Hadamard QRW and probability density function u (solution to the continuous model (5)) at time $t = 50$. Note that the peaks of the continuous model in (5) and the QRW do not match. Indeed the peaks in case of (5) spread out much faster than the discrete Hadamard QRW.*

comparing the probability mass function of discrete Hadamard QRW with a solution to (5). We observe something rather remarkable, we notice that the dynamics of the PDE model (5) which are labeled as "Continuous Model" in Figure 2 spreads out much faster than the dynamics of the discrete Hadamard QRW which are labeled as "Quantum Walk" in Figure 2. Toward this end we conjecture that such a behavior is due to the "negligence" of waiting time-delays between the jumps while deriving (5) even though it is unclear to us on how to account for such time-delays in the derivation as given in [8]. This will be rigorously justified using another an equivalent derivation of (5) starting from a generalized-classical random walk below.

We next discuss a second approach to derive the PDE system (5), this has been taken from [7]. This approach will further serve as a rigorous motivation for the introduction of fractional time derivative. We start with a generalized-classical random walk on a line. The probability of a walker being at position y at time s is given by:

$$p(y,s) = R(y-h)p(y-h,s-\tau) + L(y+h)p(y-h,s-\tau) \tag{6}$$

where h, τ are the spatial and time steps, R and L are the probabilities of the walker jumping to either right or left. In case of (5), $R(y) - L(y) = \tanh(y)$. Letting $R(y) + L(y) = 1$ yields $R(y) = \frac{1+\tanh(y)}{2}$ and $L(y) = \frac{1-\tanh(y)}{2}$. By applying appropriate Taylor expansion to (6), and by taking the limit as $h, \tau \to 0$ one arrives at (5), we refer [7] for details.

Clearly the derivation of (5) using the generalized-random walk does not account for jump-delays and as a result we arrive at the standard time derivative. We further recall from our experiment in Figure 2 that the dynamics of (5) needs to be slowed down in order to match the dynamics of discrete Hadamard QRW. With this goal in mind we recall from section 3 that the a time-delays in a random leads to (limiting system) the fractional time derivative of order $\alpha \in (0, 1)$.

Our point of departure is the generalized-classical random walk (6). By introducing the time-delays, subsequently fractional time derivative in the limit, we can approximate the discrete Hadamard QRW better. This is quite natural because a fractional time derivative is associated with time delays in the random walk. The time delays are described by a probability distribution that behaves like $\mathcal{O}(d^{-(1+\alpha)})$ for large time delays, denoted d. By introducing time delays, the following fractional PDE can be derived from the generalized-classical random walk (6):

e check what
ne delay actu-

{fracmodel}

$$\begin{aligned} \partial_s^\alpha u &= \frac{\partial^2}{\partial y^2} u - \frac{\partial}{\partial y}\left[\tanh(y) u\right] \quad \text{in } (0,\infty)\times\mathbb{R} \\ u(0,y) &= \delta(y), \quad y \in \mathbb{R} \\ \lim_{y\to\pm\infty} u(s,y) &= 0, \quad s \in (0,\infty). \end{aligned} \tag{7}$$

We refer to [7, Sec. 3] for a derivation of the time fractional Fokker Planck equation from random walks with time-delays. The same process has been applied to (7). The main difference between (7) and (5) is the Caputo fractional time derivative ∂_t^α of order $\alpha \in (0, 1)$. We refer to (4) for the definition of ∂_t^α. We also recall that when $\alpha = 1$ then $\partial_s^\alpha = \partial_s$, i.e., (5) is a special case of our fractional model (7). Due to the fact that fractional time derivative is associated to time-delays we expect a better match between the solution to (7) and discrete Hadamard QRW.

ctional Model

5. Solving The Fractional Model. To numerically solve the PDE in (7), we consider the problem

ded_problem}

$$\begin{aligned} \partial_t^\alpha u &= \frac{\partial^2}{\partial x^2} u - \frac{\partial}{\partial x}\left[\tanh(x) u\right] \quad \text{in } (0,T)\times\left(-\frac{L}{2},\frac{L}{2}\right) \\ u(0,x) &= \delta(x), \quad x \in \left(-\frac{L}{2},\frac{L}{2}\right) \\ u(t,\pm L/2) &= 0, \quad t \in (0,T). \end{aligned} \tag{8}$$

Here, the problem in (8) is the same as (7) except with a bounded domain $(0,T)\times\Omega = (0,T)\times(-\frac{L}{2},\frac{L}{2})$. The value $T > 0$ denotes the final time and L denotes the length of the spatial interval. Because we are working on a finite interval, we need to impose boundary conditions on the PDE. We choose homogeneous Dirichlet boundary conditions at $x = \pm\frac{L}{2}$, i.e. $u\left(t, \pm\frac{L}{2}\right) = 0$. Since $\lim_{x\to\infty} u(t,x) = 0$ in (7), using homogenous Dirichlet boundary conditions with L large will approximate the original boundary conditions in (7) well.

In order to numerically solve (8), we break up the scheme into a few steps. First, we approximate the initial conditions the the PDE. Next, we use a spectral method for the

spatial discretization and use a finite difference scheme for the discretization in time.

For the initial condition, we use a Dirac sequence to approximate the Dirac delta function. A Dirac sequence $\delta_n(x)$ satisfy the following two properties [6, Sec. 8.7]:

$$\int_{-\infty}^{\infty} \delta_n(x)\,\mathrm{d}x = 1, \text{ for all } n \in \mathbb{N}$$

$$\lim_{n\to\infty} \int_{-\infty}^{\infty} \delta_n(x) f(x)\,\mathrm{d}x = f(0). \tag{9}$$

The initial condition is then defined as

$$\delta(x) = \lim_{n\to\infty} \delta_n(x).$$

Taking n large will approximate the Dirac delta initial condition. We let $\delta_n(x)$ to be

$$\delta_n(x) = \begin{cases} 0, & x \le \frac{2}{n} \\ \frac{2n}{3} + \frac{n^2}{3}x, & -\frac{2}{n} < x \le -\frac{1}{n} \\ \frac{n}{3}, & \frac{-1}{n} < x \le \frac{1}{n} \\ \frac{2n}{3} - \frac{n^2}{3}x, & \frac{1}{n} < x \le \frac{2}{n} \\ 0, & \frac{2}{n} < x. \end{cases} \tag{10}$$

Figure 3 gives three $\delta_n(x)$ from our Dirac Sequence(10). By Lemma 1 and Theorem 2 in Appendix A, this choice of approximation satisfies the desired properties in (9). An additional property is that our Dirac sequence is piecewise linear, which means that the trapezoid rule for numerical quadrature will be exact for a small enough spatial mesh. Finally, given a spatial mesh size of h, we choose n so that $\frac{1}{n} > h$, which means a piecewise linear interpolation can represent the initial condition approximation exactly.

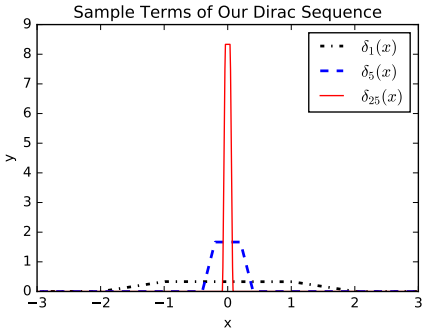

FIG. 3. *Dirac sequence from* (10)

For the spatial discretization, we utilize a spectral method. In particular, we use the sine transform the incorporate the homogenous Dirichlet boundary conditions. By taking the sine transform with respect to the spatial variable x, (7) becomes

$$\partial_t^\alpha \mathcal{F}_s\{u\} = -\frac{\pi^2\omega^2}{2L^2}\mathcal{F}_s\{u\} + \frac{\pi\omega}{L}\mathcal{F}_c\{\tanh(x)u\}, \tag{11}$$

where $\mathcal{F}_s\{u\}$ is the sine transform of u, ω is the frequency variable, and $\mathcal{F}_c\{\tanh(x)u\}$ is the cosine transform of $\tanh(x)u$. Note that $\frac{\pi\omega}{L}\mathcal{F}_c\{\tanh(x)u\} = \mathcal{F}_c\{\frac{\partial}{\partial x}[\tanh(x)u]\}$.

For the discretization in time, we use a finite difference scheme. We specifically use a $L1$ approximation scheme to approximate $\partial_t^\alpha u$ with time values $t_k = k\tau$ for $k \in \mathbb{N}$ and time step τ (c.f. [18]). The discretization is achieved by taking a backward difference approximation for u_t in (4). The resulting discretization for $\partial_t^\alpha u(t_{k+1}, x)$ is

$$\begin{aligned}\partial_t^\alpha u(t_{k+1},x) &\approx \frac{1}{\Gamma(1-\alpha)}\sum_{\ell=0}^{k}\int_{t_\ell}^{t_{\ell+1}}\frac{[u(t_{\ell+1},x)-u(t_\ell,x)]/\tau}{(t_{k+1}-y)^\alpha}dy \\ &= \frac{1}{\Gamma(2-\alpha)}\sum_{\ell=0}^{k}\frac{u(t_{\ell+1},x)-u(t_\ell,x)}{\tau^\alpha}a_{k-\ell} \end{aligned} \tag{12}$$

where $a_{k-\ell} = (k+1-\ell)^{1-\alpha} - (k-\ell)^{1-\alpha}$.

To attain a solution to our PDE, we apply the $L1$ scheme to the sine transformed PDE to produce an iterative scheme. Applying the $L1$ scheme to the left hand side of (11), we get

$$\frac{1}{\Gamma(2-\alpha)}\sum_{\ell=0}^{k}\frac{\hat{u}_{\ell+1}-\hat{u}_\ell}{\tau^\alpha}a_{k-\ell} = -\frac{\pi^2\omega^2}{2L^2}\hat{u}_{k+1} + \frac{\pi\omega}{L}\mathcal{F}_c\{\tanh(x)u_{k+1}\} \tag{13}$$

where $\hat{u}_k$ denotes the sine transform of u at time step t_k. By isolating $\hat{u}_{k+1}$ in (13), we arrive at the following equation

$$\hat{u}_{k+1} = C_2\left[\frac{\pi\omega}{L}\mathcal{F}_c\{\tanh(x)u_{k+1}\} + C_1\left(\hat{u}_k - \sum_{\ell=0}^{k-1}(\hat{u}_{\ell+1}-\hat{u}_\ell)a_{k-\ell}\right)\right] \tag{14}$$

where $C_1 = \left(\Gamma(2-\alpha)\tau^\alpha\right)^{-1}$ and $C_2 = \left(C_1 + \frac{\pi^2\omega^2}{2L^2}\right)^{-1}$.

Since $\mathcal{F}_c\{\tanh(x)u_{k+1}\}$ is on the right hand side, we use a fixed point iteration is then used to solve for u_{k+1} at every time iteration. Algorithm 1 implements the nested fixed point iteration and give us the numerical solution to (8). The outer iteration is the time evolution while the inner iteration is the fixed point iteration.

Algorithm 1 Nested FPI

$C_1 \leftarrow \left(\Gamma(2-\alpha)\tau^\alpha\right)^{-1}$
$C_2 \leftarrow \left(C_1 + \frac{\pi^2\omega^2}{2L^2}\right)^{-1}$
for $k = \{1, \dots, K\}$ **do**
  $u_{k+1,\,0} \leftarrow u_k$
  while $|u_{k+1,\,j+1} - u_{k+1,\,j}|/|u_{k+1,\,j}| > \epsilon$ **do**
    $\hat{f}_{k+1,\,j} \leftarrow \frac{\pi\omega}{L}\mathcal{F}_c\{\tanh(x)u_{k,\,j}\}$
    $\hat{u}_{k+1,\,j+1} \leftarrow C_2\left[\hat{f}_{k+1,\,j} + C_1\left(\hat{u}_k - \sum_{\ell=0}^{k-1}(\hat{u}_{\ell+1}-\hat{u}_\ell)a_{k-\ell}\right)\right]$
    $u_{k+1,\,j+1} \leftarrow \mathcal{F}_s^{-1}\{\hat{u}_{k+1,\,j+1}\}$
  end while
  $u_{k+1} \leftarrow u_{k+1,\,j+1}$
end for
return $\{u_1, \dots, u_K\}$

:Convergence

6. Convergence of Numerical Scheme. The authors in [8] provide an analytical solution to (5), which is a special case of our model with $\alpha = 1$. We know the analytical solution for (5), so we conduct numerical experiments to check for the rate of convergence of the method. This is not a proof of convergence but provides a ceh that our computations are producing reasonable results. To test for convergence, we solved the PDE in (5) on the domain $\Omega = (0, 10) \times (-200, 200)$. For the rate of convergence in time, we refine the mesh in time and compute the L^2 error while holding the spatial mesh size constant. Likewise for the spatial rate of convergence, we refine the mesh in space and compute the L^2 error while holding the time mesh size constant. Figure 4 demonstrates the convergence with respect to time refinements on the subdomain $(2, 10) \times (-200, 200)$. The subdomain $(2, 10) \times (-200, 200)$ is shown because the method does not seem to converge on the whole domain $(0, 10) \times (-200, 200)$. This is due to the irregularity of the initial condition, which hurts the convergence of the method close to the initial time. On the subdomian $(2, 10) \times (-200, 200)$, the rate of convergence is approximately 1. This is consistent with the fact that the $L1$ scheme is the same as the Backward Euler scheme for $\alpha = 1$. Figure 4 demonstrates the convergence with respect to space refinements on $(0, 10) \times (-200, 200)$.The method is approximately first order with respect to spatial refinements. Spectral methods usually exhibit a high rate of convergence, but the irregular initial conditions cause the lower rate of convergence in our case.

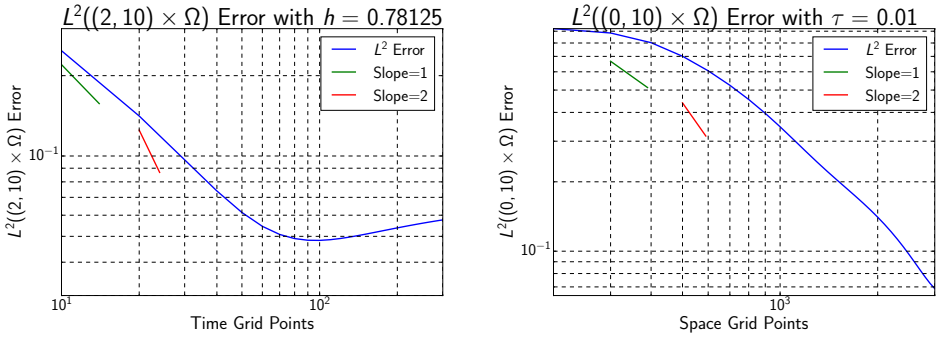

errorplot

FIG. 4. *The left figure is the L^2 norm on the subdomain $(2, 10) \times \Omega$ with respect to time refinements and the right figure is the L^2 norm on the subdomain $(0, 10) \times \Omega$ with respect to space refinements. We can see that the L^2 error converges at a rate approximately 1 with respect to time and space refinements.*

The numerical experiment discussed was for $\alpha = 1$. For values of α other than 1, the regularity of the solution to (7) may be worse, which will give a slower rate of convergence. For example, the time fractional heat equation, $\partial_t^\alpha u = u_{xx}$, can have solutions with that are not continuously differentiable with respect to time [27]. The Dirac delta initial condition further While an error analysis of the $L1$ scheme for the time fractional heat equation exists for initial conditions that are $L^2(\Omega)$ [17], more work must be done on error estimates for initial conditions not in $L^2(\Omega)$, like in our case.

Optimization

7. Optimization Method to Calculate α. Figure 5 depicts cumulative probability distributions for the QRW, the model from [8], and our fractional model. For the QRW, we calculate the cumulative probabilities by summing up individual probabilities up to the specific spatial value in the plot. For the two continuous models, the cumulative probability is calculated using a trapezoid method. As seen in Figure 5,

the fractional model with $\alpha = .75$ provides a much more accurate depiction of the QRW and is a significant improvement over the model in [8]. The choice of $\alpha = .75$

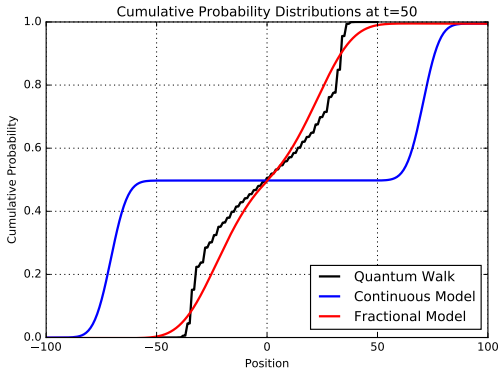

FIG. 5. *Cumulative Probability Distributions of the QRW, regular model from [8], and the fractional model with* $\alpha = .75$.

cumulativeplot

was arbitrary. We'll devote the next section to the optimization algorithm that will determine the best choice for α.

As mentioned previously, there was a large discrepancy between the continuous model from [8] and the QRW (c.f. Figure 5). Our original motivation for introducing the fractional derivative was to overcome this discrepancy. We have now introduced the fractional model and have seen the improved fit for when $\alpha = .75$, but the choice of α was arbitrary. One way to decide α would be to optimize for the fit of the QRW with respect to α. By choosing the optimal α, we will have a much clearer picture of how exactly the fractional model fits the QRW. The approach we will use has been previously utilized for finding the optimal order of the fractional Laplacian in [26].

We want to find the optimal α such that we have the best fit between the QRW and the fractional PDE model. The Hadamard QRW is discrete in space and our PDE model is continuous in space, so the notion of best fit should be the best fit between cumulative distributions. Another aspect to consider is the domain of definition for α. The fractional model in (7) assumes that $0 < \alpha < 1$. To make sure that an optimization process stays within $0 < \alpha < 1$, we add an additional term to the functional we will be minimizing. This additional term will be convex and have asymptotes at $\alpha = 0$ and $\alpha = 1$ to ensure that an optimization process stays within $0 < \alpha < 1$. The resulting functional we will be minimizing is

efunctional}

$$J[\alpha] = \frac{1}{2}\int_0^T \int_\Omega (u_\alpha - q)^2 \, \mathrm{d}x\mathrm{d}t + \gamma \frac{1}{(1-\alpha)\alpha} \tag{15}$$

where u_α is the cumulative probability distribution of the solution to our fractional PDE model with the derivative order α and q is the linear interpolant of the QRW cumulative probability distribution. The far right term will prevent the optimization process from going outside the interval $(0, 1)$, with $0 < \gamma << 1$. This will ensure that our optimization stays inside the domain of definition for the fractional PDE model. With a small γ our optimization will be most influenced by the first term, which measures how good the fit of u_α is to q.

To minimize the functional in (15), we employ a gradient descent method. In order to use the gradient descent, we need an approximation for the gradient of J. Using a

right hand Riemann sum approximation with space and time step sizes h, τ for the integral, the approximation of the gradient for (15) is

onalgradient}

$$J'[\alpha] = h\tau \sum_i \sum_j \left[(u_\alpha(t_i, x_j) - q(t_i, x_j)) \frac{d}{d\alpha} u_\alpha(t_i, x_j) \right] + \gamma \frac{2\alpha - 1}{(1-\alpha)^2 \alpha^2}, \tag{16}$$

where $\frac{d}{d\alpha} u_\alpha(t_i, x_j)$ denotes a backwards difference approximation of the derivative of $u_\alpha(t_i, x_j)$ with respect to α. The resulting gradient descent algorithm in Algorithm 2 is how we minimize the functional in (15).

Algorithm 2 Gradient Descent

1: set tolerance tol
2: initialize λ
3: initialize an initial guessα
4: compute $J'[\alpha]$
5: **while** $|J'[\alpha]| >$ tol **do**
6: $\quad \alpha \leftarrow \alpha - \lambda J'[\alpha]$
7: $\quad$ compute new $J'[\alpha]$
8: **end while**
9: **return** α

adientdescent

Another key addition to Algorithm 2, is to conduct two passes of the gradient descent. The first pass will be on a coarse mesh, specifically $h, \tau = .2$ and $\lambda = 1$. The optimal α from this first pass will give us a good initial guess for the optimal α for the second pass. The second pass will be on a finer mesh, specifically $h, \tau = .1$ and $\lambda = .5$. Additionally, the tolerance is set to be 10^{-4}.

ation Results

8. Optimization Results. After applying the prescribed optimization routine for different values for T, the following table lists the corresponding optimal α values.

T	10	20	30	40	50	60	70	80	90
Optimal α	0.645	0.701	0.724	0.742	0.754	0.763	0.771	.776	.781

TABLE 1
Optimal α values at differing T values

optimizationresults

One observation from Table 1 is that our original guess of $\alpha = .75$ was relatively accurate. Another observation is that α is increasing for increasing T. Figure 6 depicts the fractional model with $\alpha = .781$ compared to the QRW at different time values. We can see that the optimization algorithm has provided a value for α that matches the QRW closely, which is an improvement over the previous model.

s:Conclusion

9. Conclusions and Future Work. To summarize, we first noted a large discrepancy between the discrete QRW and the continuous model from [8]. To enrich the model from [8], we introduced a fractional derivative in time. We provided a numerical method to approximate the solution to the fractional model and provided an optimization algorithm to choose the order of the fractional derivative that would best fit the discrete QRW. Our results show that the introduced fractional model is a an improvement over the previous continuous model in the literature. As a result, we have introduced the first continuous model that can model discrete QRW dynamics

write more in conclusion and recall to reader why they should care

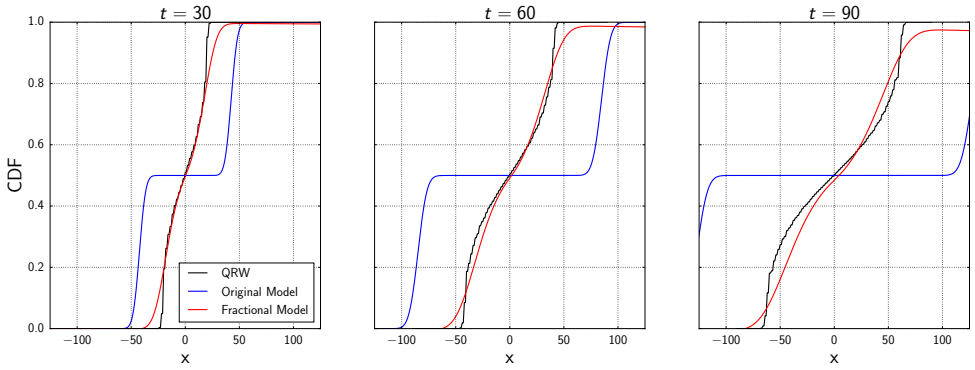

FIG. 6. *Comparison of CDFs from the QRW and the fractional model with the optimal α value from when $T = 90$*

resultsT90

effectively. Future work involves an analysis of the numerical scheme for the fractional problem and analysis of the optimization problem and the numerical scheme to solve it.

Acknowledgments. We would like to thank Marco Lanzagorta for introducing us to the topic of Quantum Random Walks. We would also like to thank Salvador Venegas-Andraca for providing us helpful comments and feedback on this paper.

Appendix A. Proof that our Dirac Sequence in (10) Satisfies the Properties in (9). For our Dirac sequence in (10) to satisfy the properties in (9), we need every element of the sequence to integrate to 1. In the limit, we want the Dirac sequence integrated against a continuous function f to concentrate the integral on the value $f(0)$. The first Lemma gives us the first condition.

equence_proof

tegral_lemma

LEMMA 1. *Let δ_n be defined as in (10). Then,*

$$\int_{-\infty}^{\infty} \delta_n(x)\mathrm{d}x = 1.$$

Proof. Every element of the sequence is a trapezoid with base lengths $\frac{4}{n}, \frac{2}{n}$ and height $\frac{n}{3}$. The area of this trapezoid is 1 for all n. ∎

The Lemma shows that δ_n integrates to 1, but it will also be helpful in showing that δ_n satisfies the next property.

irac_theorem

THEOREM 2. *Let $f : \mathbb{R} \to \mathbb{R}$ be continuous at $x = 0$ and let δ_n be defined as in (10). Then,*

$$\lim_{n\to\infty} \int_{-\infty}^{\infty} \delta_n(x)f(x)\mathrm{d}x = f(0).$$

Proof. Let $f : \mathbb{R} \to \mathbb{R}$ be continuous at $x = 0$. By Lemma 1,

$$\begin{aligned}\lim_{n\to\infty} \left| \int_{-\infty}^{\infty} \delta_n(x)f(x)\mathrm{d}x - f(0) \right| &= \lim_{n\to\infty} \left| \int_{-\frac{2}{n}}^{\frac{2}{n}} \delta_n(x)(f(x) - f(0))\mathrm{d}x \right| \\ &\leq \lim_{n\to\infty} \int_{-\frac{2}{n}}^{\frac{2}{n}} \left| \delta_n(x)(f(x) - f(0)) \right| \mathrm{d}x.\end{aligned}$$

∎

By the Cauchy-Schwarz inequality,

$$\lim_{n\to\infty}\int_{-\frac{2}{n}}^{\frac{2}{n}}\left|\delta_n(x)(f(x)-f(0))\right|\mathrm{d}x \le \lim_{n\to\infty}\int_{-\frac{2}{n}}^{\frac{2}{n}}\left|f(x)-f(0)\right|\mathrm{d}x\int_{-\frac{2}{n}}^{\frac{2}{n}}\left|\delta_n(x)\right|\mathrm{d}x.$$

By Lemma 1, $\int_{-\frac{2}{n}}^{\frac{2}{n}}\delta_n(x)\mathrm{d}x = 1$, so we have

$$\lim_{n\to\infty}\int_{-\frac{2}{n}}^{\frac{2}{n}}\left|f(x)-f(0)\right|\mathrm{d}x\int_{-\frac{2}{n}}^{\frac{2}{n}}\left|\delta_n(x)\right|\mathrm{d}x \le \lim_{n\to\infty}\frac{4}{n}\max_{|x|\le\frac{2}{n}}|f(x)-f(0)|$$

Because f is continuous, $\max_{|x|<\frac{2}{n}}|f(x)-f(0)| \to 0$ as $n\to\infty$, and

$$\lim_{n\to\infty}\left|\int_{-\infty}^{\infty}\delta_n(x)f(x)\mathrm{d}x - f(0)\right| = 0.$$

REFERENCES

[1] N. Abatangelo and E Valdinoci. Getting acquainted with the fractional laplacian. *arXiv:1710.11567v1*, 2017.

[2] A. Ambainis. Quantum walk algorithm for element distinctness. *SIAM Journal on Computing*, 37(1), 2007.

[3] H. Antil and S. Bartels. Spectral approximation of fractional PDEs in image processing and phase field modeling. *Comput. Methods Appl. Math.*, 17(4):661–678, 2017.

[4] H. Antil and D. Leykekhman. A brief introduction to pde constrained optimization. *To appear: IMA Volume*, 2018.

[5] H. Antil and C.N Rautenberg. Sobolev spaces with non-muckenhoupt weights, fractional elliptic operators, and applications. *arXiv preprint arXiv:1803.10350*, 2018.

[6] G. Arfken. *Mathematical Methods for Physicists*. Academic Press Inc., 3rd edition, 1985.

[7] E. Barkai, R. Metzler, and J. Klafter. From continuous time random walks to the fractional fokker-planck equation. *Physical Review Letters*, 61(1), 2000.

[8] Ph. Blanchard and M.-O. Hongler. Quantum random walks and piecewise deterministic evolution. *Physical Review Letters*, 92(12), 2004.

[9] T. Brown, S. Du, H. Eruslu, and F.-J. Sayas. Analysis of models for viscoelastic wave propagation. *arXiv preprint arXiv:1802.00825*, 2018.

[10] A. Bueno-Orovio, D. Kay, V. Grau, B. Rodriguez, and K. Burrage. Fractional diffusion models of cardiac electrical propagation: role of structural heterogeneity in dispersion of repolarization. *Journal of Royal Society Interface*, 2014.

[11] L. Caffarelli and L. Silvestre. An extension problem related to the fractional Laplacian. *Comm. Partial Differential Equations*, 32(7-9):1245–1260, 2007.

[12] C. Calatroni, C. Chung, J.C. De Los Reyes, C.B. Schonlieb, and T. Valkonen. Bilevel approaches for learning of variational imaging models. *arXiv:1505.02120v1*, 2015.

[13] A. Childs. Universal computation by quantum walk. *Physical Review Letters*, 102, 2009.

[14] A. Childs. On the relationship between continuous- and discrete-time quantum walk. *Communications in Mathematical Physics*, 294(2), 2010.

[15] National Science Foundation. The quantum leap: Leading the next quantum revolution. 2018. https://www.nsf.gov/news/special_reports/big_ideas/quantum.jsp.

[16] C. Gal and M. Warma. Fractional-in-time semilinear parabolic equations and applications.

[17] B.T. Jin, R. Lazarov, and Z. Zhou. An analysis of the l1 scheme for the subdiffusion equation with nonsmooth data. *IMA Journal of Numerical Analysis*, 36(1), 2016.

[18] Y. Lin and C. Xu. Finite difference/spectral approximations for the time-fractional diffusion equation. *Journal of Computational Physics*, 225, 2007.

[19] N.B. Lovett, S. Cooper, M. Everitt, M. Trevers, and V. Kendon. Universal quantum computation using the discrete-time quantum walk. *Physical Review A*, 81, 2010.

[20] R. Metzler and J. Klafter. The random walk's guide to anomalous diffusion: a fractional dynamics approach. *Physics Reports*, 339(1), 2000.

[21] S.A. Molˇ canov and E. Ostrovskiĭ. Symmetric stable processes as traces of degenerate diffusion processes. *Teor. Verojatnost. i Primenen.*, 14:127–130, 1969.

2hitchhikers [22] E. Di. Nezza, G. Palatucci, and E. Valdinoci. Hitchhikers guide to the fractional sobolev spaces. *Bulletin des Sciences Mathématiques*, 136(5):521–573, 2012.

samko_1993 [23] S.G. Samko, A.A. Kilbas, and O.I. Marichev. *Fractional integrals and derivatives: theory and applications*. Gordon and Breach Science Publishers, 1993.

shenvi_2003 [24] N. Shenvi, J. Kempe, and K.B. Whaley. Quantum random-walk search algorithm. *Physical Review A*, 67, 2003.

shor [25] P. Shor. Polynomial-time algorithms for prime factorization and discrete logarithms on a quantum computer. *SIAM Journal on Computing*, 26(5), 1997.

valdinoci_opt [26] J. Sprekels and E. Valdinoci. A new type of identification problems: Optimizing the fractional order in a nonlocal evolution equation. *SIAM Journal on Control and Optimization*, 55(1), 2017.

stynes [27] M. Stynes. Too much regularity may force too much uniqueness. *arXiv:1607.01955v1*, 2016.

valdinoci [28] E. Valdinoci. From the long jump random walk to the fractional laplacian. *arXiv:0901.3261*, 2009.

ersypen_2001 [29] L.M. Vandersypen, M. Steffen, G. Breyta, C.S. Yannoni, M.H. Sherwood, and I.L. Chuang. Experimental realization of shor's quantum factoring algorithm using nuclear magnetic resonance. *Nature*, 414(6866), 2001.

venegas [30] E. Venegas-Andraca. Quantum walks: a comprehensive review. *Quantum Information Processing*, 2012.